2020-05

Effects of fullerene C60 in blue mussels: Role of mTOR in autophagy related cellular/tissue alterations

Sforzini, S

http://hdl.handle.net/10026.1/16272

10.1016/j.chemosphere.2019.125707
Chemosphere
Elsevier BV

Effects of fullerene C_{60} in blue mussels: role of mTOR in autophagy related cellular/tissue alterations

Susanna Sforzini [a], Caterina Oliveri [a], Audrey Barranger [b], Awadhesh N. Jha [b], Mohamed Banni [c], Michael N. Moore [b, d, e], Aldo Viarengo [f]

[a] Department of Sciences and Technological Innovation (DiSIT), University of Piemonte Orientale "A. Avogadro", V.le T. Michel 11, 15121 Alessandria, Italy

[b] School of Biological and Marine Sciences, University of Plymouth, Drake Circus, Plymouth, PL4 8AA, UK

[c] Laboratory of Biochemistry and Environmental Toxicology, ISA, Chott-Mariem, Sousse, Tunisia

[d] European Centre for Environment & Human Health (ECEHH), University of Exeter Medical School, Truro, TR1 3HD, UK

[e] Plymouth Marine Laboratory, Plymouth, PL1 3DH, UK

[f] Institute for the study of Anthropic impacts and Sustainability in marine environment - National research Council (CNR-IAS), Via de Marini 6, 16149 Genova, Italy

Corresponding author:

Aldo Viarengo

IAS-CNR

Via De Marini 6, 16149 Genova, Italy

Phone: +393357182939

E-mail: aldo.viarengo@ias.cnr.it

Abstract

The effects of C_{60} on mTOR (mechanistic Target of Rapamycin) activity in mussel digestive gland were investigated. mTOR is a kinase that senses physiological and environmental signals to control eukaryotic cell growth. mTOR is present in two complexes: the phosphorylated mTORC1 regulates cell growth by activating anabolic processes, and by inhibiting catabolic processes (i.e. autophagy); mTORC2 also modulates actin cytoskeleton organization. Mussels were exposed to C_{60} (0.01, 0.1 and 1 mg/L) for 72h. Immunocytochemical analysis using a specific antibody revealed the cellular distribution of C_{60} in mussel digestive gland, already at the lowest concentration. In exposed mussels, the dephosphorylation of mTORC1 and mTORC2 may explain the C_{60} effects, i.e. the reduction of lysosomal membrane stability, the enhancement of LC3B protein, and the increase of lysosomal/cytoplasmic volume ratio; as well the cytoskeletal alterations. No oxidative stress was observed. Multivariate analysis was used to facilitate the interpretation of the biomarker data. Finally, a low density oligo-microarray was used to understand the cellular responses to fullerene. Transcriptomics identified a number of differentially expressed genes (DEGs) showing a maximum in animals exposed to 0.1 mg/L C_{60}. The most affected processes are associated with energy metabolism, lysosomal activity and cytoskeleton organization. In this study, we report the first data on the subcellular distribution of C_{60} in mussel's cells; and on the involvement of mTOR inhibition in the alterations due to nanoparticle accumulation. Overall, mTOR deregulation, by affecting protein synthesis, energy metabolism and autophagy, may reduce the capacity of the organisms to effectively grow and reproduce.

Keywords: mussel, mTOR, fullerene C_{60}, autophagy, cytoskeleton, transcriptomics

1. Introduction

The fullerenes represent one major class of carbon-based nanoparticles (NPs) (Khan et al., 2017) that exist naturally (e.g. in geological materials), are generated incidentally (e.g. from combustion processes) and are produced in large quantities as engineered nanomaterials (Buseck et al., 1992; Nielsen et al., 2008). Fullerenes are widespread in all ecosystems (surface waters -Emke et al., 2015 and Farré et al. 2010; atmospheric aerosols -Sanchís et al., 2012; soils -Sanchís et al. 2013; sediments -Sanchís et al. 2015) and, with the further development of nanotechnology, their environmental concentration is continuously increasing (Benn et al., 2012; Pycke et al., 2012). There is however lack of information with respect to mechanisms of actions of these materials for hazard and risk assessment, in particular, in the marine environment.

In the fullerene family, C_{60} (buckminsterfullerene) is the most abundant representative. Its unique characteristics render C_{60} and its derivatives promising candidates for various applications in different fields such as medicine and electronics (Urbaszek et al., 2017).

C_{60} has been demonstrated to act as a “free radical sponge” with an antioxidant efficacy hundreds of times greater than conventional antioxidants (Krusic et al., 1991; Liu et al., 2014). However, somewhat paradoxically, C_{60} is also able to generate reactive oxygen species (ROS) by light excitation (Trpkovic et al., 2012). This dual property of fullerene C_{60} (both pristine as well derivatized) molecules, and their bioaccumulation capacity, have given rise to numerous studies aimed at clarifying whether these particles may represent a risk to animal and human health (Goodarzi et al., 2017; Trpkovic et al., 2012).

Studies about the toxicity of fullerene toward vertebrates and invertebrates has highlighted that these particles exert ROS-mediated and/or ROS-independent adverse effects depending on various factors (e.g. physicochemical properties, target cells and tissues, type of exposure) (Canesi et al., 2010; Goodarzi et al., 2017; Oberdörster, 2004; Ringwood et al., 2009; Trpkovic et al., 2012). Although the modes of toxic action are not yet fully understood, several studies have indicated

induction and perturbation of autophagy as an emerging mechanism of fullerene (and more in general of nanomaterials) cellular pathophysiology (Stern et al., 2012; Zabirnyk et al., 2007). Many studies have demonstrated nanomaterial-induced lysosomal dysfunctions (Stern et al., 2012). In particular, fullerene was shown to induce a reduction of lysosomal membrane stability (LMS) in marine bivalve molluscs, which are organisms widely used in environmental biomonitoring (Canesi et al., 2010; Dallarés et al., 2018; Maisano et al., 2017; Moore et al., 2009; Ringwood et al., 2009; Sanchís et al., 2018; Viarengo et al., 2007). Destabilisation of lysosomal membranes represents a cellular pathological reaction known to be linked to both augmented and dysfunctional autophagy (Moore et al, 2006).

Macroautophagy is an essential, conserved process that results in the degradation of cytoplasmic components (protein aggregates, organelles, etc.) in lysosomes (Cuervo, 2004; Klionsky and Emr, 2000). Autophagy, both macro- and microautophagy, is crucial for cell homeostasis and survival under both normal and stress conditions; as well is implicated in many relevant diseases (Levine and Kroemer, 2008). One of the key regulators of autophagy is mTOR (mechanistic Target of Rapamycin), an evolutionarily conserved serine/threonine kinase that plays a pivotal role in the regulation of cell growth and metabolism in response to different stimuli, such as nutrients, hormones and stressors (Dobashi et al., 2011; Huang and Fingar, 2014; Saxton and Sabatini, 2017; Soulard et al., 2009).

The aim of this research was to study the effects of C_{60} on mTOR activity and related lysosomal perturbations in the digestive gland or hepatopancreas of blue mussels (*M. galloprovincialis* Lam). mTOR exists in two functionally distinct complexes: namely mTOR complex 1 (mTORC1) and mTOR complex 2 (mTORC2) (Copp et al., 2009; Wullschleger et al., 2006). In particular, the phosphorylated form of mTORC1 regulates cell growth by activating anabolic processes (i.e. transcription, ribosome biogenesis, protein synthesis, etc.), and by inhibiting catabolic processes (such as autophagy); mTORC2 also modulates actin cytoskeleton organization (Saxton and

Sabatini, 2017; Soulard et al., 2009). Tissue C_{60} intracellular accumulation and subcellular distributions were evaluated by immunofluorescence using a specific antibody. Changes in the phosphorylation of mTOR were investigated by an immunocytochemical approach. To study the possible consequences of mTOR dephosphorylation on digestive gland physiology, we analysed LMS and the expression of the protein LC3B (as biomarkers of the autophagic process), lysosomal/cytoplasmic (L/C) volume ratio (revealing excessive levels of autophagy), lysosomal neutral lipid (mainly triglyceride) accumulation (index of lipid metabolic disorders) and lipofuscin accumulation (oxidative stress biomarker); while the changes in cytoskeletal actin/tubulin structures were also evaluated. Previous studies have shown that for lysosomal/autophagic and oxidative stress biomarker data, Principal Component Analysis (PCA) coupled with Hierarchical Cluster Analysis can be used as an indicator of homeostasis or health in cellular systems (Moore, 2010; Moore et al., 2015; Sforzini et al., 2018a). In this investigation, PCA and cluster analysis were used to integrate multi-biomarker data; and to test this as a potential predictive model for cellular patho-physiological function against functional damage in the lysosomes of mussel hepatopancreatic digestive cells (Sforzini et al., 2018a). Finally, due to the relevance of transcriptomic data to understanding the cellular adaptive responses to environmental stressors, a recently developed and validated low density oligo-microarray (465 genes, suitable to follow 15 stress response pathways) was used (Banni et al., 2017; Sforzini et al., 2018b). Transcription of selected genes was verified by RT-qPCR.

2. Materials and methods

2.1. Chemicals and organisms

Chemicals of analytical grade were purchased from Sigma-Aldrich Co. (UK/Italy), unless otherwise indicated. Adult *Mytilus galloprovincialis* Lam. (45-50 mm) sampled from the intertidal zone at Trebarwith Strand, Cornwall, UK, a relatively pristine reference site (50° 38’ 40" N, 4° 45’ 44" W)

were maintained under laboratory conditions prior to the experiments as described previously by Barranger et al. (2019a,b).

2.2. Experimental design and sampling

After depuration, the mussels were transferred to 2-L glass beakers (containing 1.8 L of seawater) to acclimatize for 48 h. Two mussels were used per beaker. A photoperiod of 12 h light : 12 h dark was maintained throughout the experiment. Seawater oxygenation was provided and the seawater quality monitored as described by Barranger et al. (2019a). Mussels were exposed for 3 days with no water changes to 0.01, 0.1 and 1 mg/L C_{60} (fullerene suspension homogenised by ultrasonication) as described by Barranger et al. (2019a). A total of 26 individuals were used per treatment. After 3-day exposure period, mussel sex was determined (Banni et al., 2017). Digestive glands (DG) from 10 female mussels were processed for immunohistochemical and cyotochemical analysis (Sforzini et al., 2018a) as well for transcriptomics (microarray and qRT-PCR) (Banni et al., 2017). The C_{60} concentrations used in these experiments were selected taking into account previous studies (Al-Subiai et al., 2012; Di et al., 2017; Moore et al., 2009).

2.3. Immunohistochemical analysis

Frozen sections (10 µm) of mussel digestive glands obtained by using a cryostatic microtome (LeicaCM3050) were fixed in paraformaldehyde (PFA) solution (4% PFA in phosphate buffer saline-PBS, pH 7.2, 20 min at 20 ± 1 °C) (Sforzini et al., 2014).

Immunofluorescent anti-C_{60} staining was performed in accordance with the method described by Sforzini et al. (2014). In brief, fixed sections were incubated in a permeabilisation and blocking solution (0.5% Triton X-100, 2% bovine serum albumin-BSA, 0.5% rabbit serum in PBS) for 1 h at 20 ± 1 °C. Sections were rinsed and incubated with the primary antibody (monoclonal mouse anti-Fullerene antibody -Santa Cruz Biotechnology Inc., 1/100 in PBS containing 1% BSA and 0.05%

Triton X-100) at 4 °C overnight; then the secondary antibody was applied i.e. polyclonal rabbit to mouse (FITC) (Abcam) (1/100 in 1% BSA and 0.05% Triton X-100 in PBS) for 1 h at 20 ± 1 °C in the dark. After rinsing, sections were stained with DAPI (DNA-specific fluorescent probe) and mounted as described in Sforzini et al. (2014).

To reveal the possible accumulation of fullerene in the lysosomes of the digestive gland cells of C_{60} exposed mussels, immunofluorescence colocalization of fullerene and the lysosomal enzyme cathepsin D was performed following essentially the method described in Sforzini et al. (2018a).

The investigations related to mTOR alterations induced in mussel digestive gland by fullerene C_{60} involved the immunohistochemical analysis of the level of phosphorylation (activation/inhibition) of mTORC1 and mTORC2 as well the of total amount of mTOR. Taking into consideration the recent findings by Copp et al. (2009) about the different phosphorylation of mTOR when associated with mTORC1 and mTORC2 (specifically, mTORC1 contains mTOR phosphorylated predominantly on S2448, whereas mTORC2 contains mTOR phosphorylated predominantly on S2481), we used two different specific antibodies. The methods for the immunofluorescent anti-phospho- mTORC1 (by using the anti m-TOR phospho S2448 antibody, Abcam), as well mTOR staining are reported in Sforzini et al. (2018a). For the evaluation of the level of activation/inhibition of mTORC2, mussel digestive gland sections, after fixation (as described above) were incubated in a permeabilisation and blocking solution (0.5% Triton X-100, 2% BSA, 0.5% goat serum in PBS, 1 h at 20 ± 1 °C) and then with the primary antibody (anti m-TOR (phospho S2481) antibody, Abcam, 1/100 in PBS containing 1% BSA and 0.05% Triton X-100) overnight at 4 °C. Sections were then washed and the secondary antibody was applied, i.e. polyclonal goat to rabbit (Chromeo™ 488) (Abcam) (1/100 in 1% BSA and 0.05% Triton X-100 in PBS) for 1 h at 20 ± 1 °C in the dark. Finally, sections were rinsed in PBS, counterstained with propidium iodide and mounted.

Immunofluorescent anti-LC3B staining, autophagy marker microtubule-associated protein chain 3B, was performed by incubating the sections, after permeabilisation and blocking (0.5% Triton X-100, 2% BSA, 0.5% goat serum in PBS, for 1 h at 20 ± 1 °C), with the primary antibody (rabbit polyclonal to LC3B - Abcam, 1/100 in PBS containing 1% BSA and 0.05% Triton X-100, overnight at 4 °C) and then with the secondary antibody i.e. polyclonal goat to rabbit (Alexa Fluor® 488) (Abcam) (1/100 in 1% BSA and 0.05% Triton X-100 in PBS) for 1 h at 20 ± 1 °C in the dark. After rinsing, sections were stained with DAPI and mounted.

To reveal the potential link between the state of activation/inactivation of mTORC2 and the cytoskeleton structure, immunofluorescent anti-tubulin staining and F-actin staining was performed as described by Banni et al. (2017) and Sforzini et al. (2018b). Antibody to tubulin and F-actin combination staining was also performed: after the reaction for the primary antibody (see Banni et al., 2017), sections were incubated with the secondary antibody i.e. goat anti-rabbit (DyLight® 594) (Abcam) (1/100 in 1% BSA and 0.05% Triton X-100 in PBS) for 1 h at 20 ± 1 °C in the dark; sections were washed in PBS and then incubated with Green Fluorescent Phalloidin Conjugate (CytoPainter F-actin Labeling Kit-Green Fluorescence -Abcam) for 1 h at 20 ± 1 °C. After rinsing, sections were mounted.

Control sections for non-specific staining were processed without the primary or secondary antibodies: no positive stain was observed. Slides were viewed under 400 × magnification by an inverted photo-microscope (Zeiss Axiovert 100M connected to a digital camera Zeiss AxioCam MRm) equipped for fluorescence microscopy using FITC, Rhodamine and DAPI emission filters. Sections double immunolabelled for C_{60} and cathepsin D and for mTOR were viewed under 400 × magnification by Axio Observer and images were taken with ApoTome.2 (Zeiss, Germany). The obtained images were analysed by an image analysis system (Scion Image) for the quantification of the mean fluorescence intensity.

2.4. Lysosomal alterations

A set of parameters was used to evaluate the possible consequences of mTORC1 dephosphorylation induced in mussels by increasing concentrations of fullerene C_{60} on digestive gland cell physiology. The determination of the biomarkers was evaluated on cryostat digestive gland sections (10 µm) obtained as described above. The LMS (based on the latency of the lysosomal enzyme N-acetyl-β-hexosaminidase -NAH) and the L/C volume ratio (in sections reacted for NAH) were assessed as reported by Moore (1976, 1988) and by Moore and Clarke (1982), respectively. The lipofuscin content was determined using the Schmorl reaction (Moore, 1988; Pearse, 1972), and neutral lipid content by the Oil Red-O (ORO) staining (Moore, 1988). Sections were viewed under 400 × magnification by a Axiolab photo-microscope and the pictures obtained were analysed using an image analysis system (Scion Image). LMS was expressed as labilization period (min); L/C volume ratio as well lipofuscin and neutral lipid accumulations were expressed as a percentage variation with respect to controls.

2.5. Univariate statistical analysis

At least five replicates per control and per C_{60} concentration were analysed. Each replicate consists of the digestive gland from one mussel; the molluscs were sampled from different beakers. The non-parametric Mann-Whitney *U*-test was employed to compare the data from C_{60} exposed organisms with those of the controls ones.

2.6. Multivariate statistical analysis

Biomarker data for mussels treated with C_{60} fullerene were analysed using non-parametric multivariate analysis software, PRIMER v 6 (PRIMER-E Ltd., University of Aukland, New Zealand; Clarke, 1999; Clarke & Warwick, 2001). All of the biomarker data were log transformed [$\log_n(1+x)$] and standardised to the same scale. Principal component analysis (PCA) and

hierarchical cluster analysis, derived from Euclidean distance similarity matrices were used to visualise dissimilarities between sample groups. The results were further tested for significance using non-parametric analysis of similarity (PRIMER v6 - ANOSIM), which is an approximate analogue of the univariate ANOVA and reflects on differences between treatment groups in contrast to differences among replicates within samples (the *R* statistic). Under the null hypothesis H_0 ("no difference between samples"), $R = 0$, and this was tested by a non-parametric permutations approach. Using this approach, there should be little or no effect on the average R value if the labels identifying which replicates belong to which samples are randomly rearranged.

Finally, correlation coefficients for the individual biomarkers comprising the first principal component PC1 (representing integrated biomarker data) for the various experimental treatments were derived, including that for lysosomal membrane stability, which has been used previously as an integrated measure of cellular well-being (Allen and Moore, 2004; Moore et al., 2006; Sforzini et al., 2015, 2017, 2018a).

2.7. RNA isolation and Microarray hybridization

Total RNA was prepared from a digestive gland tissues according to Chomczynski and Sacchi (1987), using TRI-Reagent. A total number of 5 biological replicates (pools made of two mussels each) were considered. 5 µg of total RNA from each pool was reverse transcribed using oligodT(19)VN primer (Banni et al., 2011). Competitive dual-color microarray hybridization was carried out using the new STREM platform (Banni et al. 2017; Barranger et al., 2019b). All the procedure was conducted according to Banni et al. (2017) and Barranger et al. (2019b). Global mean normalization and Log_2 transformation was performed for each expression level as described in Banni et al. (2017). DEGs were identified by Significance Analysis of Microarray (SAM, http://statweb.stanford.edu/~tibs/SAM/).

2.8. qRT-PCR

The qRT-PCR reactions were realised using the same RNA extract as microarray hybridization. Four probes and primer pairs (tubulin, tripsin, catalase and cytosolic superoxide dismutase Table S1 - see Supplementary Information) were employed. The cDNA preparation and the Q-PCR details are as described elsewhere in details (Banni et al., 2011, 2017; Barranger et al., 2019b; Negri et al., 2013). The relative expression data were normalized against ribosomal protein riboL27 (AJ625928), an invariant actin isotype (AJ625116), and 18S rRNA (L33452). Statistical analyses were performed on the group mean values using a random reallocation test (Pfaffl et al., 2002).

3. Results

3.1. Immunohistochemical and cytochemical analysis

The concentrations of C_{60} utilised in this study did not provoke any mortality (data not shown) in *M. galloprovincialis* after 3 d of exposure; the results demonstrate that C_{60} accumulated in the digestive gland of molluscs induced, even at the lowest dose, significant changes of mTOR activation with negative consequences on cellular and tissue physiology (Fig. 1-4).

Western blot (WB) is often used as a complementary assay to confirm antibody specificity in immunohistochemistry (IHC) and provide more quantitative analysis of protein levels. However, the epitope recognized by the primary antibody may not be identically available in WB and IHC assays (www.cellsignal.co.uk); in the case of phosphoproteins (as mTOR), the phosphate could be hydrolysed by phosphatases released during the sample preparation. For these reasons, in this study, we decided to use immunohistochemistry to evaluate by specific antibodies the protein expression/level of phosphorylation in cryostat sections that are suitable for maintaining the cellular characteristics and the structure of native proteins.

Immunohistochemical analysis of digestive gland sections of mussels exposed to C_{60} using a specific anti-fullerene antibody showed a positive reaction (Fig. 1B-D); no staining was observed in

control animals (Fig. 1A). Co-localization of fullerene and the lysosomal enzyme cathepsin D by double immunofluorescence labelling demonstrated the accumulation of C_{60} inside lysosomes (Fig. 1F). Quantification of the C_{60} fluorescence signal by digital imaging (Fig. 1E) showed a significant increase in fluorescence intensity in mussels exposed to all the concentrations, with respect to controls; and a plateau was reached at the lowest dose (10 µg/L). No statistically significant difference was observed among the different C_{60} concentrations.

Immunofluorescence labelling of mussel digestive gland sections with the two different antibodies to phospho-mTOR (phosphorylated on S2448 -mTORC1, and on S2481 -mTORC2) was positive in control animals (Fig. 2A, panels 1, 2). The respective signals were differentially located, mainly in the perinuclear region of the tubule epithelial cells for mTORC1 (Fig. 2E, panel 1); and generally in the cytoplasm for mTORC2 (Fig. 2E, panel 2). The immunocytochemical data demonstrated that all the different concentrations of C_{60} induced a strong dephosphorylation of mTOR (for both S2448 and S2481), with respect to the controls (Fig. 2B, C, D, F - panels 1, 2). When the digestive gland tissue sections were reacted for the mTOR antibody in order to reveal the protein level, the fluorescent signal in C_{60} exposed mussels showed no change when compared to controls (Fig. S1 – see Supplementary Information); as for phospho-mTOR, similar values were obtained in animals exposed to all the different concentrations (Fig. S1 E).

The strong inactivation (dephosphorylation) of mTOR was accompanied by pathological reactions involving the lysosomal vacuolar system, as well by cytoskeleton structural alterations. In particular, C_{60}, already at the lowest concentration (0.01 mg/L), induced a strong decrease of LMS in digestive gland cells (Fig. 3A), associated with an increase in the expression of the protein LC3 (autophagy marker microtubule-associated protein chain 3B - LC3B) (Fig. 3C); a significant enhancement of L/C volume ratio, revealing an injury at the cell and tissue level, was also observed (+ 49%, with respect to controls) (Fig. 3B). Fullerene caused an alteration of fatty acid metabolism in mussels: we found in the lysosomes a significant accumulation (lipidosis) of neutral lipids, which

was greater at the lowest concentration (0.01 mg/L) (+ 84%, with respect to controls) (Fig. 3D). However, no oxidative stress was generated in the digestive gland cells of C_{60} exposed mussels, as demonstrated by the results of lysosomal lipofuscin content, which showed no change compared to the controls (Fig. 3E). The investigations related to the possible negative consequences of C_{60} exposure on the cytoskeleton involved the immunofluorescent analysis of tubulin, as well the fluorescent staining of F-actin. As shown in Fig. 4, both of these cytoskeletal components presented strong alterations in mussels exposed at all the different C_{60} concentrations. In particular, even at the lowest dose (10 µg/L), a rearrangement was observed of the tubulin structure, with the presence of highly stained cytoplasmic granules containing the protein. When the digestive gland sections were stained for F-actin, in C_{60} exposed mussels the cytoskeletal architecture of the digestive tubules was strongly affected, with the alterations in the actin component of the cytoskeleton being particularly evident in the cortical compartment of the cells.

3.2. Multivariate analysis of biomarker reactions

Principal component (PCA) and hierarchical cluster analysis of all the biomarker reactions showed that C_{60} had a significant detrimental effect on the digestive cells of mussels (Fig. 5); and that the first principal component (PC1) captured 69.6% of the variation. Analysis of similarity shows that the controls were significantly different from the treatments (ANOSIM, global R Statistic: $R = 0.512$, $P \leq 0.01$). Treatments with the three concentrations of C_{60} were clearly separated from the control ($P < 0.01$). Only C_{60} 0.01 mg/L and C_{60} 0.1 mg/L showed a significant difference within the C_{60} treatments ($P < 0.05$; Fig. 5). Table 1 shows that some of the correlation coefficients in the linear combinations of biomarkers making up PC1 were statistically significant, including lysosomal membrane stability, lysosomal lipid, phosphorylated mTORC1 (p-mTORC1 active form) and lysosomal-cytoplasmic volume ratio.

3.3. Transcriptomic analysis

In order to compare the expression patterns of genes in response to increasing fullerene concentrations compared to controls, a cDNA microarray with available annotated gene sequences from *M. californianus*, *M. galloprovincialis*, *M. edulis*, and *C. gigas* containing 465 probes was used. Based on the enriched GO functional annotation, target genes were selected to explore 6 distinct biological processes related to the stress response in bivalve molluscs, including translation, carbohydrate metabolism, mitochondrial activities, lysosomal activity, proteolysis and cytoskeletal organisation. Transcriptomic analysis identified a number of DEGs (differentially expressed genes) showing a maximum of 87 DEGs in animals exposed to 0.1 mg/L C_{60} (Table 2; Figure 6). The resulting expression profiles identified a total of 113 differentially expressed genes (DEGs) in at least one condition (Fig. 6). Of the 113 DEGs, 28 genes were found to be in common in the three experimental conditions. Comparative analysis showed differences in gene expression level in mussels exposed to 0.1 mg/L C_{60} with the maximum DEGs number related to translation and cytoskeletal organization (Fig. 7).

3.4. Confirmation analysis

We performed a qRT-PCR to refine and confirm the relative expression levels of four genes belonging to the most important biological processes, including the genes encoding trypsin (proteolysis), tubulin (cytoskeleton), catalase and cytosolic superoxide dismutase (oxidative stress). Microarray and qRT-PCR data indicated a positive relationship in all cases (Fig. S2, see Supplementary Information).

4. Discussion

The effects of fullerene C_{60} on mTOR (mechanistic target of rapamycin) were investigated with particular emphasis on the potential consequences of its deregulation on intracellular lysosomal

autophagy in digestive gland/hepatopancreatic cells in blue mussels (*M. galloprovincialis*). The digestive gland was chosen for the analysis as it is the organ devoted to food absorption and digestion (Bayne, 2009); as well to the accumulation and detoxification of toxic contaminants (Al-Subiai et al., 2012; Banni et al., 2016; Barranger et al., 2019a,b; Di et al., 2017; Gomes et al., 2012; Moore et al., 2007; Sforzini et al., 2018a,b; Viarengo et al., 1981). Moreover, digestive gland has been identified as a relevant target for nanoparticle accumulation and effects (Al-Subiai et al., 2012; Barranger et al., 2019a,b; Canesi et al., 2012; Di et al., 2017; McCarthy et al., 2013; Tedesco et al., 2010).

Fullerene C_{60} uptake and distribution have been shown *in vitro* on various cell types using various methods (e.g. TEM/EFTEM techniques, by synthesizing fluorescent labelled fullerene, by immunostaining - Franskevych et al., 2017; Grebinyk et al., 2018; Porter et al., 2007; Raoof et al., 2012; Ringwood et al., 2009; Russ et al., 2016). *In vivo* studies have largely focused on identifying the uptake capacity of different organs and tissues (Bullard-Dillard et al., 1996; Sumner et al., 2015; Tervonen et al., 2010). To the best of our knowledge, this is the first study that demonstrated the *in vivo* intracellular accumulation and the subcellular distribution of C_{60} in tissue sections of fullerene exposed organisms. The immunocytochemical analysis, using a specific anti-fullerene C_{60} antibody, enabled the localisation of C_{60} in the digestive tubule epithelial cells; while the double fluorescent labelling with the antibody against cathepsin D (a highly conserved lysosomal protease; Phillips et al., 2006) showed that fullerene is actually sequestered in secondary lysosomes. Rather unexpectedly, immunofluorescence data showed that the maximum uptake of $C_{60}$was achieved in mussels exposed at the lowest concentration (10 µg/L). Immunofluorescent anti-C_{60} staining reaction was performed following a methodology (recently developed by Sforzini et al., 2014) that allows the localization of contaminants (such as B[*a*]P and TCDD) within tissues of animals exposed to low chemical concentrations (Banni et al., 2016; Sforzini et al., 2018a, 2018b).

Chemical analytical results for the molluscan digestive glands, sampled in the same experiment

(Barranger et al., 2019), are fully supportive of the immunocytochemical fluorescence analysis. Fullerene accumulated in the digestive gland of C_{60} treated mussels did not show any significant change among the different doses (0.01, 0.1, 1 mg/L). Previously reported investigations have clearly demonstrated that in mussels exposed to 0.1 and 1 mg/L C_{60}, the digestive gland represents a relevant site of chemical accumulation (Al-Subiai et al., 2012; Di et al., 2017).

Fullerene exposure caused a marked inhibition of mTOR. This serine/threonine protein kinase plays an essential role in regulating cell growth and division in response to various factors such as nutrients, hormones and environmental stressors (Dobashi et al., 2011; Huang and Fingar, 2014; Saxton and Sabatini, 2017; Soulard et al., 2009). mTOR is found in two distinct evolutionarily conserved signalling complexes: mTOR complex 1 (mTORC1) regulates cell growth and metabolism; and mTOR complex 2 (mTORC2) also plays a role in the regulation of the actin cytoskeleton organization (Dobashi et al., 2011). The dephosphorylation (inhibition) of mTOR kinase in both mTOR complexes has been shown to cause an enhancement of the autophagic activity, a decrease in protein synthesis, reduced mitochondrial activity (mTORC1) and cytoskeletal perturbations (mTORC2) (Rispal et al., 2015; Saxton and Sabatini, 2017; Soulard et al., 2009; Wullschleger et al., 2006). A recent study (Copp et al., 2009) showed that mTOR kinase is phosphorylated differentially for mTORC1 and mTORC2: specifically mTORC1 containing mTOR phosphorylated predominantly on S2448, whereas mTORC2 contains mTOR phosphorylated predominantly on S2481. Our group has recently demonstrated the perinuclear distribution of mTORC1 (by the use of anti-mTOR phospho S2448) inside the digestive gland cells of mussels (Sforzini et al., 2018a). This study has demonstrated that even the lowest C_{60} concentration provoked a dramatic dephosphorylation of mTORC1. The results of this study indicate important linkages between mTORC1 inhibition and the alterations observed in the lysosomal system, particularly the destabilisation of the lysosomal membranes (often an indicator of induced autophagic activity), as well as the increase of L/C volume ratio that reveal excessive levels of

autophagy (i.e. catabolism of the macromolecules not compensated for by protein synthesis) (Levine and Kroemer, 2008; Moore and Viarengo, 1987; Moore et al., 2008a). The observed increase in autophagic activity was further substantiated by the enhanced expression of the LC3 protein (autophagy marker microtubule-associated protein chain 3B - LC3B), one of the most widely used biomarkers for autophagy (Fig. 3C; Chen et al., 2013; Kast and Dominguez, 2017). In addition, in the digestive gland of mussels exposed to all C_{60} concentrations, there was enhancement of lysosomal neutral lipid/triglyceride accumulation (lipidosis). This cytopathological reaction may be related to impairment of fatty acid utilization for energy generation by mitochondria, and the consequent autophagic sequestration of cytosolic lipids in the lysosomal vacuolar system (Morita et al., 2015). However, no change was observed in the lysosomal content of lipofuscins, a significant end product of oxidative attack on lipids and proteins, and a useful biomarker of moderate and severe oxidative stress (Moore, 2008; Viarengo, 1989). These results are in general agreement with previous *in vivo* studies in molluscs, demonstrating that, in organisms exposed to C_{60} under light photoperiod, oxidative stress does not appear to play a primary role in the toxicity of fullerenes at low, environmentally relevant exposures. C_{60} treatment for 24 h at 1-5 mg/L caused limited effects on lipofuscin accumulation (Canesi et al., 2010); while no change was found in lipid peroxidation levels in the digestive glands of oysters treated for 4 days with C_{60} at 1-500 μg/L (Ringwood et al., 2009). Moreover, in conjunction with the cellular data, no relevant transcriptional changes were recorded for genes involved in oxidative stress response in digestive gland cells after exposure to the three fullerene concentrations (CAT and SOD - Fig. S2, see Supplementary Information). Principal Component Analysis (PCA) is an effective method for reducing the multi-dimensionality of biomarker data and integrating this data into a “health status space” (Allen and Moore, 2004; Chatfield and Collins, 1980). Previous models have shown that there is a direct relationship between LMS, as an indicator of cellular health, and the first principal component (PC1) of other combined biomarker reactions (Allen & Moore, 2004; Moore et al., 2006; Sforzini et al., 2015,

2017, 2018a). This use of PC1 as a measure of health status space is clearly demonstrated in this work, where a strong correlation with lysosomal membrane stability is indicated (Table 1), from the correlation coefficients for the biomarkers comprising PC1 (integrated biomarker data). However, the autophagy-related biomarkers, lysosomal/cytoplasmic volume ratio and inhibition of mTORC1, were also important influences in the first principal component as an holistic indicator of cellular health, discriminating between controls and C_{60} exposed mussels (Table 1). Lysosomal lipid showed a weaker correlation (but still significant) with the first principal component (Table 1), while lipofuscin was not significantly correlated (Table 1), hence, supporting the conclusions above that oxidative stress was not significantly induced by C_{60} treatment.

The transcriptomic response showed a bell-shaped trend in the total number of genes analysed. This finding highlighted that, in the digestive gland, there was an increase of the DEGs involved in the reaction to C_{60} increasing concentrations (0.01 - 0.1 mg/L); however, at the highest concentration (1 mg/L), the transcriptomic response tended to decrease; probably related to the adverse effects of C_{60} being accumulated more rapidly. Although the number of DEGs between the lowest and highest concentration are similar, it should be noted that 0.01 mg/L C_{60} exhibited an higher number of DEGs related to energy metabolism and 1 mg/L C_{60} induced a stronger response in the DEGs related to translation and proteolysis.

The transcriptomic data may help to clarify how the digestive gland cells react to C_{60}. The results of the microarray analysis indicate that, among the DEGs involved in the energy metabolism (carbohydrate metabolism and mitochondrial activity), the higher percent is down-regulated (Table S2 - see Supplementary Information). This is the typical metabolic change associated with mTORC1 dephosphorylation, such as a reduction of the energy resources of the cells. In line with the effects of C_{60} on mTOR inhibition, it is the net increase of the up-regulated DEGs related to the lysosomal activity (Table S2). Interpretation of the biological implications of the DEGs related to protein synthesis are more difficult to explain. The DEGs involved in the translation process show

the maximum at the intermediate C_{60} concentration (0.1 mg/L); however, the balance between up- and down-regulated genes changes in the mussels exposed to the different C_{60} concentrations, this making the interpretation of the data more complicated. Nevertheless, these results show that the enhanced lysosomal autophagic activity is not compensated for by a significant increase in the transcription of the mRNA involved in the translation process. Furthermore, in the same animals, we observed a significant increase of the L/C volume ratio: an indication that the cells had a catabolic status.

Nanoparticles, on entry into cells, are known to induce perturbations in the cytoplasmic organization; and, consequently of the cytoskeletal network (Ispanixtlahuatl-Meráz et al., 2018). In previous investigations (Al-Subiai et al., 2012; Di et al., 2017), mussels exposed to C_{60} at 0.1 and 1 mg/L either alone or in combination with polycyclic aromatic hydrocarbons (PAHs) showed a loss in definition of the digestive tubules. The phosphorylated active form of mTORC2 regulates the actin cytoskeletal organization (Dobashi et al., 2011; Rispal et al., 2015). In this study, the immunohistochemical fluorescent labelling of control mussel digestive gland sections by the use of an anti-mTOR antibody phosphorylated on S2481 (mTORC2) highlighted an immunopositive reaction, the fluorescent staining being mainly located in the cytoplasm of the tubule epithelial cells: other studies (on yeast, protozoa and mammalian cells) localized mTORC2 mainly in the cytoplasm (Barquilla et al., 2008; Betz and Hall, 2013; Kunz et al., 2000). Immunofluorescent reaction demonstrated a strong decrease in dephosphorylated mTORC2 in mussels treated with C_{60}, even at the lowest fullerene concentration. This result may explain, at least in part, the pathological disorganisation of the actin cytoskeleton structures observed in digestive gland tubules of C_{60} exposed mussels. Microtubules, together with actin filaments and intermediate filaments, are the main cytoskeletal structures in eukaryotic cells: the microtubule network is involved in various physiological functions, such as cell movement, intracellular protein trafficking, and mitosis (Fletcher and Mullins, 2010; Parker et al., 2014). Our immunocytochemical results showed a

striking rearrangement of the microtubular network, characterised by the presence of strongly stained tubulin containing granules in the cytoplasm (Fig. 3C & 4). The formation of granules containing tubulin has previously been demonstrated in cells from stressed organisms (Banni et al., 2016, 2017; Clark and Shay, 1981; Martin et al., 2010; Sforzini et al., 2018b). Part of the free tubulin may be also trapped on the surface of stress granules, as recently reported by Shao et al.(2017). Microtubules undergo continual disassembly and reassembly within the cell, and the synthesis of tubulin is known to be autoregulated on the basis of the amount of cytosolic unpolymerized monomer (Gasic and Mitchison, 2019). The decrease in the amount of free tubulin monomer should stimulate the protein neo synthesis in order to maintain the cytoskeletal organisation essential for cellular physiological functions such as vesicle movements and autophagy. Cytoskeletal organisation was one of the main contributing biological processes in the cytopathological reaction to fullerene as depicted by the microarray data. Tubulin was among the genes showing an increasing trend over the three C_{60} concentrations, probably to compensate for the observed alteration of this crucial cytoskeletal component of the cell.

Our data show that C_{60} accumulation in the digestive gland cells reaches a plateau in the animals treated with the lowest fullerene concentration. Actin filaments provide the mechanical capability for many cellular activities that involve membrane deformation, such as cell motility, phagocytosis, endocytosis and cytokinesis (Kast and Dominguez, 2017). mTORC2 inhibition (i.e. dephosphorylation) affects actin organisation, as well as endocytosis (Riggi et al., 2019; Rispal et al., 2015). A possible explanation of our results is that in the C_{60} treated mussels, the endocytotic (pinocytotic) uptake of nanoparticles tends to decrease, possibly related to mTORC2 dephosphorylation. Inhibition of mTORC1 also may contribute to the decrease in endocytotic capacity (Flinn & Backer, 2010).

It is also important to mention that C_{60} did not affect the overall cellular concentration of mTOR protein: the amount of the protein as well as the mRNA coding for mTOR did not show any change

in the animals exposed to the various fullerene concentrations. These results highlight that mTOR phosphorylation / dephosphorylation mechanism is a key element in the patho-physiological regulation of mussel cellular metabolism.

5. Conclusions

In this study, we report the first published data on the subcellular distribution of C_{60} fullerene in mussel digestive gland cells; and on the possible involvement of mTOR inhibition (as part of the mTORC1/mTORC2 complexes) in the patho-physiological perturbations induced by nanoparticle accumulation. C_{60} fullerene provokes an excessive induction of autophagy, as shown by higher lysosomal activity and the enhancement of the expression of the protein LC3B; as well an increased lysosomal-cytoplasmic volume ratio (L/C volume). However, no supporting evidence for C_{60}-induced oxidative stress was observed, although the absence of enhanced lipofuscin does not rule out the possibility of mild oxidative stress. These findings seem to indicate that moderate to severe ROS production and oxidative damage are not necessary under these conditions to inhibit the mTOR pathways. Autophagic induction by C_{60} (as for other nanoparticles - Stern et al., 2012; Zabirnyk et al., 2007) may represent an attempted degradation in lysosomes of material that is recognised by the cell as foreign or aberrant, such as pathogens or damaged intracellular proteins and membranes. We have demonstrated the accumulation of C_{60} fullerene in the lysosomal-vacuolar system of the major digestive gland epithelial cells (i.e. digestive cells). Excessive autophagy may also be involved in the process of perturbation of cytoskeletal structures (Monastyrska et al., 2009; Zheng et al., 2018). However, nanoparticles, within the cells, may themselves cause an alteration in the cytoskeletal network (Ispanixtlahuatl-Meráz et al., 2018). Although the possible relationships between mTORC1 and mTORC2, as well the factors that inhibit mTORC2, are not fully elucidated, the cytoskeletal alterations induced by C_{60} may impair the growth of the cells and their organisation in the tubules of the digestive gland. Overall, dysregulation of mTORC1 & 2 may reduce the

capacity of the cells, and organisms, to properly grow and reproduce. Consequently, mTOR dephosphorylation should be considered a diagnostic biomarker for the toxic effects of the C_{60} and polycyclic aromatic hydrocarbons as previously demonstrated (Sforzini et al., 2018a); and, under chronic stressful conditions, prognostic for potential harmful effects at the whole animal and population level. These new findings confirm and clarify why a decrease in LMS is indicative of the larger phenomenon related to mTOR inhibition that may lead to a reduction in the physiological scope for growth of the animals (Allen and Moore, 2004).

Acknowledgements

This study was supported financially by Natural Environment Research Council (NERC), UK (Grant No.NE/L006782/1; PI: ANJ).

References

Allen, J.I., Moore, M.N., 2004. Environmental prognostics: is the current use of biomarkers appropriate for environmental risk evaluation. Mar. Environ. Res. 58, 227-232.

Al-Subiai, S.N., Arlt, V.M., Frickers, P.E., Readman, J.W., Stolpe, B., Lead, J.R., Moody, A.J., Jha, A.N., 2012. Merging nano-genotoxicology with eco-genotoxicology: an integrated approach to determine interactive genotoxic and sub-lethal toxic effects of $C_{(60)}$ fullerenes and fluoranthene in marine mussels, *Mytilus* sp. Mutat. Res. 745, 92-103.

Banni, M., Negri, A., Mignone, F., Boussetta, H., Viarengo, A., Dondero, F., 2011. Gene expression rhythms in the mussel *Mytilus galloprovincialis* (Lam.) across an annual cycle. PLoSOne 6 (5), e18904.

Banni, M., Sforzini, S., Balbi, T., Corsi, I., Viarengo, A., Canesi, L., 2016. Combined effects of n-TiO2 and 2,3,7,8-TCDD in *Mytilus galloprovincialis* digestive gland: a transcriptomic and immunohistochemical study. Environ. Res. 145, 135-144.

Banni, M., Sforzini, S., Arlt, V.M., Barranger, A., Dallas, L.J., Oliveri, C., Aminot, Y., Pacchioni, B., Millino, C., Lanfranchi, G., Readman, J.W., Moore, M.N., Viarengo, A., Jha, A.N., 2017. Assessing the impact of Benzo[a]pyrene on Marine Mussels: Application of a novel targeted low density microarray complementing classical biomarker responses. PLoS One 12(6):e0178460. doi: 10.1371/journal.pone.0178460.

Barquilla, A., Crespo, J.L., Navarro M., 2008. Rapamycin inhibits trypanosome cell growth by preventing TOR complex 2 formation. Proc. Natl. Acad. Sci. USA 105, 14579-14584.

Barranger, A., Langan, L.M., Sharma, V., Rance, G.A., Aminot Y., Weston, N.J., Akcha, F., Moore, M.N., Arlt, V.M., Khlobystov, A.N., Readman, J.W., Jha, A.N., 2019a. Antagonistic Interactions between Benzo[a]pyrene and Fullerene (C_{60}) in Toxicological Response of Marine Mussels. Nanomaterials (Basel). 9(7). pii: E987. doi: 10.3390/nano9070987.

Barranger, A., Rance, G.A., Aminot, Y., Dallas, L.J., Sforzini, S., Weston, N.J., Banni, M., Arlt, V.M., Moore, M.N., Readman, J.W., Viarengo, A., Khlobystov, A.N., Jha, A, N., 2019b. An integrated approach to determine interactive genotoxic and global gene expression effects of multiwalled carbon nanotubes (MWCNTs) and Benzo[a]pyrene (BaP) on marine mussels: Evidence of reverse 'Trojan Horse' effects. Nanotoxicology 13, 1324-1343; https://doi.org/10.1080/17435390.2019.1654003.

Bayne, B.L., 2009. Marine Mussels: Their Ecology and Physiology. Cambridge University Press 528 p.

Benn, T., Herckes, P., Westerhoff, P., 2012. Chapter 9 - Fullerenes in Environmental Samples: C_{60} in Atmospheric Particulate Matter, in: Farré, M., Barceló, D. (Eds.), Analysis and Risk of

Nanomaterials in Environmental and Food Samples. Elsevier B.V., vol. 59, pp. 291-303. https://doi.org/10.1016/B978-0-444-56328-6.00010-4.

Betz, C., Hall, M. N., 2013. Where is mTOR and what is it doing there? J. Cell Biol. 203, 563-574.

Bullard-Dillard, R., Creek, K.E., Scrivens, W.A., Tour, J.M., 1996. Tissue Sites of Uptake of ^{14}C-Labeled C60. Bioorg. Chem. 24, 376-385.

Buseck, P.R., Tsipursky, S.J., Hettich, R., 1992. Fullerenes from the Geological Environment. Science 257, 215-217.

Canesi, L., Fabbri, R., Gallo, G., Vallotto, D., Marcomini, A., Pojana, G., 2010. Biomarkers in *Mytilus galloprovincialis* exposed to suspensions of selected nanoparticles (Nano carbon black, C_{60} fullerene, Nano-TiO_2, Nano-SiO_2). Aquat. Toxicol. 100, 168-177.

Canesi, L., Ciacci, C., Fabbri, R., Marcomini, A., Pojana, G., Gallo, G., 2012. Bivalve molluscs as a unique target group for nanoparticle toxicity. Mar. Environ. Res. 76, 16-21.

Chatfield, C., Collins, A. J., 1980. Introduction to multivariate analysis. London: Chapman and Hall.

Chen, S., Jiang, Y.Z., Huang, L., Zhou, R.J., Yu, K.D., Liu, Y., Shao, Z.M., 2013. The residual tumor autophagy marker LC3B serves as a prognostic marker in local advanced breast cancer after neoadjuvant chemotherapy. Clin. Cancer Res. 19, 6853-6862.

Chomczynski, P., Sacchi, N., 1987. Single-step method of RNA isolation by acid guanidinium thiocyanate-phenol-chloroform extraction. Anal. Biochem. 162: 156-169.

Clarke, K.R., 1999. Non-metric multivariate analysis in community-level ecotoxicology. Environ. Toxicol. Chem. 18, 117-127.

Clark, M.A., Shay, J.W., 1981. The role of tubulin in the steroidogenic response of murine adrenal and rat Leydig cells. Endocrinology 109, 2261-2263.

Clarke, K.R., Warwick, R.M., 2001. Change in marine communities: an approach to statistical analysis and interpretation. PRIMER-є, Plymouth, UK.

Copp, J., Manning, G., Hunter, T., 2009. TORC-specific phosphorylation of mammalian target of rapamycin (mTOR): phospho-Ser2481 is a marker for intact mTOR signaling complex 2. Cancer Res. 69, 1821-1827.

Cuervo, A.M., 2004. Autophagy: in sickness and in health. TRENDS Cell Biol. 14, 70-77.

Dallarés, S., Carrasco, N., Álvarez-Muñoz, D., Rambla-Alegre, M., Solé, M., 2018. Multibiomarker biomonitoring approach using three bivalve species in the Ebro Delta (Catalonia, Spain). Environ. Sci. Pollut. Res. Int. 25, 36745-36758.

Di, Y., Aminot, Y., Schroeder, D.C., Readman, J.W., Jha, A.N., 2017. Integrated biological responses and tissue-specific expression of *p53* and *ras* genes in marine mussels following exposure to benzo(α)pyrene and C_{60} fullerenes, either alone or in combination. Mutagenesis 32, 77-90. doi: 10.1093/mutage/gew049.

Dobashi, Y., Watanabe, Y., Miwa, C., Suzuki, S., Koyama, S., 2011. Mammalian target of rapamycin: a central node of complex signaling cascades. Int. J. Clin. Exp. Pathol. 4, 476-495.

Emke, E., Sanchís, J., Farré, M., Bäuerlein, P.S., de Voogt P., 2015. Determination of several fullerenes in sewage water by LC HR-MS using atmospheric pressure photoionization. Environ. Sci. Nano 2, 167-176.

Farré, M., Pérez, S., Gajda-Schrantz, K., Osorio, V., Kantiani, L., Ginebreda, A., Barceló, D., 2010. First determination of C_{60} and C_{70} fullerenes and N-methylfulleropyrrolidine C_{60} on the suspended material of wastewater effluents by liquid chromatography hybrid quadrupole linear ion trap tandem mass spectrometry. J. Hydrol. 383, 44-51.

Fletcher DA, Mullins RD, 2010. Cell mechanics and the cytoskeleton. Nature. 463, 485-492.

Flinn, R.J., Backer, J.M., 2010. mTORC1 signals from late endosomes: taking a TOR of the endocytic system. Cell Cycle 9, 1869-1870.

Franskevych, D., Palyvoda, K., Petukhov, D., Prylutska, S., Grynyuk, I., Schuetze, C., Drobot, L., Matyshevska, O., Ritter, U., 2017. Fullerene C_{60} Penetration into Leukemic Cells and Its Photoinduced Cytotoxic Effects. Nanoscale Res. Lett. 12:40.

Gasic, I., Mitchison, T.J., 2019. Autoregulation and repair in microtubule homeostasis. Curr. Opin. Cell. Biol. 56, 80-87. doi: 10.1016/j.ceb.2018.10.003.

Gomes, T., Pereira, C.G., Cardoso, C., Pinheiro, J.P., Cancio, I., Bebianno, M.J., 2012. Accumulation and toxicity of copper oxide nanoparticles in the digestive gland of *Mytilus galloprovincialis*. Aquat. Toxicol. 118-119, 72-79.

Goodarzi, S., Da Ros, T., Conde, J., Sefat, F., Mozafari, M., 2017. Fullerene: biomedical engineers get to revisit an old friend. Mater. Today 20, 460-480.

Grebinyk, A., Grebinyk, S., Prylutska, S., Ritter, U., Matyshevska, O., Dandekar, T., Frohme, M., 2018. C_{60} fullerene accumulation in human leukemic cells and perspectives of LED-mediated photodynamic therapy. Free Radic. Biol. Med. 124, 319-327.

Huang, K., Fingar, D.C., 2014. Growing knowledge of the mTOR signaling network. Semin. Cell Dev. Biol. 36, 79-90.

Ispanixtlahuatl-Meráz, O., Schins, R.P.F., Chirino, Y.I., 2018. Cell type specific cytoskeleton disruption induced by engineered nanoparticles. Environ. Sci. Nano. 5, 228-245.

Kast, D.J., Dominguez, R., 2017. The Cytoskeleton-Autophagy Connection. Curr. Biol. 27, R318-R326.

Khan, I., Saeed, K., Khan, I., 2017. Nanoparticles: Properties, applications and toxicities. Arab. J. Chem., Available online 18 May 2017. https://doi.org/10.1016/j.arabjc.2017.05.011.

Klionsky, D. J., Emr, S. D., 2000. Autophagy as a regulated pathway of cellular degradation. Science 290, 1717-1721.

Krusic, P.J., Wasserman, E., Keizer, P.N., Morton, J.R., Preston, K.F., 1991. Radical reactions of c60. Science 254, 1183-1185.

Kunz, J., Schneider, U., Howald, I., Schmidt, A., Hall, M.N., 2000. HEAT repeats mediate plasma membrane localization of Tor2p in yeast. J. Biol. Chem. 275, 37011-37020.

Levine, B., Kroemer, G., 2008. Autophagy in the pathogenesis of disease. Cell. 132, 27-42.

Liu, Q., Cui, Q., Li, X.J., Jin, L., 2014. The applications of buckminsterfullerene C_{60} and derivatives in orthopaedic research. Connect. Tissue Res. 55, 71-79.

Maisano, M., Cappello, T., Natalotto, A., Vitale, V., Parrino, V., Giannetto, A., Oliva, S., Mancini, G., Cappello, S., Mauceri, A., Fasulo, S., 2017. Effects of petrochemical contamination on caged marine mussels using a multi-biomarker approach: Histological changes, neurotoxicity and hypoxic stress. Mar. Environ. Res. 128, 114-123.

Martin, D., Duarte, M., Lepault, J., Poncet, D., 2010. Sequestration of free tubulin molecules by the viral protein NSP2 induces microtubule depolymerisation during rotavirus infection. J. Virol. 84, 2522-2532.

McCarthy, M.P., Carroll, D.L., Ringwood, A.H., 2013. Tissue specific responses of oysters, *Crassostrea virginica*, to silver nanoparticles. Aquat. Toxicol. 138-139, 123-128.

Monastyrska, I., Rieter, E., Klionsky, D.J., Reggiori, F., 2009. Multiple roles of the cytoskeleton in autophagy. Biol. Rev. Camb. Philos. Soc. 84, 431-448.

Moore, M.N., 1976. Cytochemical demonstration of latency of lysosomal hydrolases in digestive gland cells of the common mussel *Mytilus edulis*, and changes induced by thermal stress. Cell Tissue Res. 175, 279-287.

Moore, M.N., 1988. Cytochemical responses of the lysosomal system and NADPH-ferrihemoprotein reductase in molluscan digestive cells to environmental and experimental exposure to xenobiotics. Mar. Ecol. Prog. Ser. 46, 81-89.

Moore, M.N., 2008. Autophagy as a second level protective process in conferring resistance to environmentally-induced oxidative stress. Autophagy 4, 254-256.

Moore, M.N., 2010. Is toxicological pathology characterised by a loss of system complexity? Mar. Environ. Res. 69, S37-S41.

Moore, M.N., Clarke, K.R., 1982. Use of microstereology and cytochemical staining to determine the effects of crude oil-derived aromatic hydrocarbons on lysosomal structure and function in a marine bivalve mollusc *Mytilus edulis*. Histochem. J. 14, 713-718.

Moore, M.N., Viarengo, A., 1987. Lysosomal membrane fragility and catabolism of cytosolic proteins: evidence for a direct relationship. Experientia 43, 320-323.

Moore, M.N., Allen, J.I., McVeigh, A., 2006. Environmental prognostics: an integrated model supporting lysosomal stress responses as predictive biomarkers of animal health status. Mar. Environ. Res., 61, 278-304.

Moore, M.N., Viarengo, A., Donkin, P., Hawkins, A.J., 2007. Autophagic and lysosomal reactions to stress in the hepatopancreas of blue mussels. Aquat. Toxicol. 84, 80-91.

Moore, M.N., Koehler, A., Lowe, D., Viarengo, A., 2008. Lysosomes and autophagy in aquatic animals, in: Klionsky, D. (Ed.), Methods in Enzymology. Academic Press/Elsevier, Burlington, pp. 582-620.

Moore, M.N., Readman, J.A.J., Readman, J.W., Lowe, D.M., Frickers, P.E., Beesley, A., 2009. Lysosomal cytotoxicity of carbon nanoparticles in cells of the molluscan immune system: an *in vitro* study. Nanotoxicology 3, 40-45.

Moore, M.N., Shaw, J.P., Ferrar Adams, D.R., Viarengo, A., 2015. Anti-oxidative cellular protection effect of fasting-induced autophagy as a mechanism for hormesis. Mar. Environ. Res. 107, 35-44.

Morita, M., Gravel, S.P., Hulea, L., Larsson, O., Pollak, M., St-Pierre, J., Topisirovic, I., 2015. mTOR coordinates protein synthesis, mitochondrial activity and proliferation. Cell Cycle 14, 473-480.

Negri, A., Oliveri, C., Sforzini, S., Mignione, F., Viarengo, A., Banni, M., 2013. Transcriptional response of the mussel *Mytilus galloprovincialis* (Lam.) following exposure to heat stress and copper. PLoS One 8(6):e66802.

Nielsen, G.D., Roursgaard, M., Jensen, K.A., Poulsen, S.S., Larsen, S.T. 2008. *In vivo* biology and toxicology of fullerenes and their derivatives. Basic Clin. Pharmacol. Toxicol. 103, 197-208.

Oberdörster, E., 2004. Manufactured nanomaterials (fullerenes, C_{60}) induce oxidative stress in the brain of juvenile largemouth bass. Environ. Health Perspect. 112, 1058-1062.

Oberdörster, E., Zhu, S., Blickley, T.M., McClellan-Green, P., Haasch, M.L., 2006. Ecotoxicology of carbon-based engineered nanoparticles: Effects of fullerene (C_{60}) on aquatic organisms. Carbon 44, 1112-1120.

Parker, A.L., Kavallaris, M., McCarroll, J.A., 2014. Microtubules and their role in cellular stress in cancer. Front. Oncol. 4, 153.

Pearse, A.G.E., 1972, third ed. Histochemistry Theoretical and Applied, vol. 2 Churchill Livingstone, Edinburgh and London. 1518 pp.

Pfaffl, M.W., Horgan, G.W., Dempfle, L., 2002. Relative expression software tool (REST©) for group-wise comparison and statistical analysis of relative expression results in real-time PCR. Nucleic Acids Res. 30: e36.

Phillips, S.N., Muzaffar, N., Codlin, S., Korey, C.A., Taschner, P.E., de Voer, G., Mole, S.E., Pearce, D.A., 2006. Characterizing pathogenic processes in Batten disease: use of small eukaryotic model systems. Biochim. Biophys. Acta 1762, 906-919.

Porter, A.E., Gass, M., Muller, K., Skepper, J.N., Midgley, P., Welland, M., 2007. Visualizing the uptake of C_{60} to the cytoplasm and nucleus of human monocyte-derived macrophage cells using energy-filtered transmission electron microscopy and electron tomography. Environ. Sci. Technol. 41, 3012-3017.

Pycke, B.F., Chao, T.C., Herckes, P., Westerhoff, P., Halden, R.U., 2012. Beyond nC60: strategies for identification of transformation products of fullerene oxidation in aquatic and biological samples. Anal. Bioanal. Chem. 404, 2583-2595.

Raoof, M., Mackeyev, Y., Cheney, M.A., Wilson, L.J., Curley, S.A., 2012. Internalization of C_{60} fullerenes into cancer cells with accumulation in the nucleus via the nuclear pore complex. Biomaterials 33, 2952-2960.

Riggi, M., Bourgoint, C., Macchione, M., Matile, S., Loewith, R., Roux, A., 2019. TORC2 controls endocytosis through plasma membrane tension. J. Cell Biol. 218, 2265.

Ringwood, A.H., Levi Polyachenko, N., Carroll, D.L., 2009. Fullerene exposures with oysters: embryonic, adult, and cellular responses. Environ. Sci. Technol. 43, 7136-7141.

Rispal, D., Eltschinger, S., Stahl, M., Vaga, S., Bodenmiller, B., Abraham, Y., Filipuzzi, I., Movva, N.R., Aebersold, R., Helliwell, S.B., Loewith, R., 2015. Target of Rapamycin Complex 2 Regulates Actin Polarization and Endocytosis via Multiple Pathways. J. Biol. Chem. 290, 14963-14978.

Russ, K.A., Elvati, P., Parsonage, T.L., Dews, A., Jarvis, J.A., Ray, M., Schneider, B., Smith, P.J., Williamson, P.T., Violi, A., Philbert, M.A., 2016. C_{60} fullerene localization and membrane interactions in RAW 264.7 immortalized mouse macrophages. Nanoscale 8, 4134-4144.

Sanchís, J., Berrojalbiz, N., Caballero, G., Dachs, J., Farré, M., Barceló, D., 2012. Occurrence of Aerosol-Bound Fullerenes in the Mediterranean Sea Atmosphere. Environ. Sci. Technol 46, 1335-1343. DOI: 10.1021/es200758m.

Sanchís, J., Božović, D., Al-Harb,i N.A., Silva, L.F., Farré, M., Barceló, D., 2013. Quantitative trace analysis of fullerenes in river sediment from Spain and soils from Saudi Arabia. Anal. Bioanal. Chem. 405, 5915-5923. doi: 10.1007/s00216-013-6924-z.

Sanchís, J., Oliveira, L.F., de Leão, F.B., Farré, M., Barceló, D., 2015. Liquid chromatography-atmospheric pressure photoionization-Orbitrap analysis of fullerene aggregates on surface

soils and river sediments from Santa Catarina (Brazil). Sci Total Environ. 505, 172-179. doi: 10.1016/j.scitotenv.2014.10.006.

Sanchís, J., Llorca, M., Olmos, M., Schirinzi, G.F., Bosch-Orea, C., Abad, E., Barceló, D., Farré, M., 2018. Metabolic Responses of *Mytilus galloprovincialis* to Fullerenes in Mesocosm Exposure Experiments. Environ. Sci. Technol. 52, 1002-1013.

Saxton, R.A., Sabatini, D.M., 2017. mTOR Signaling in Growth, Metabolism, and Disease. Cell. 168, 960-976.

Sforzini, S., Moore, M.N., Boeri, M., Benfenati, E., Colombo, A., Viarengo, A., 2014. Immunofluorescence detection and localization of B[*a*]P and TCDD in earthworm tissues. Chemosphere 107, 282-289.

Sforzini, S., Moore, M.N., Boeri, M., Bencivenga, M., Viarengo, A., 2015. Effects of PAHs and dioxins on the earthworm *Eisenia andrei*: A multivariate approach for biomarker interpretation. Environ. Pollut. 196, 60-71.

Sforzini, S., Moore, M., Mou, Z., Boeri, M., Banni, M., Viarengo, A., 2017. Mode of action of Cr(VI) in immunocytes of earthworms: implications for animal health. Ecotoxicol. Environ. Saf. 138, 298-308.

Sforzini, S., Moore, M.N., Oliveri, C., Volta, A., Jha, A., Banni, M., Viarengo, A., 2018a. Role of mTOR in autophagic and lysosomal reactions to environmental stressors in molluscs. Aquat. Toxicol. 195, 114-128.

Sforzini, S., Oliveri, C., Orrù, A., Chessa, G., Jha, A., Viarengo, A., Banni, M., 2018b. Application of a new targeted low density microarray and conventional biomarkers to evaluate the health status of marine mussels: A field study in Sardinian coast, Italy. Sci. Total Environ. 628-629, 319-328.

Shao, J., Gao, F., Zhang, B., Zhao, M., Zhou, Y., He, J., Ren, L., Yao, Z., Yang, J., Su, C., Gao, X., 2017. Aggregation of SND1 in Stress Granules is Associated with the Microtubule Cytoskeleton During Heat Shock Stimulus. Anat. Rec. (Hoboken) 300, 2192-2199.

Soulard, A., Cohen, A., Hall, M.N., 2009. TOR signaling in invertebrates. Curr. Opin. Cell Biol. 21, 825-836.

Stern, S.T., Adiseshaiah, P.P., Crist, R.M., 2012. Autophagy and lysosomal dysfunction as emerging mechanisms of nanomaterial toxicity. Part. Fibre Toxicol. 9, 20.

Sumner, S.C., Snyder, R.W., Wingard, C., Mortensen, N.P., Holland, N.A., Shannahan, J.H., Dhungana, S., Pathmasiri, W., Han, L., Lewin, A.H., Fennell, T.R., 2015. Distribution and biomarkers of carbon-14 labeled fullerene C_{60} ([^{14}C(U)]C_{60}) in female rats and mice for up to 30 days after intravenous exposure. J. Appl. Toxicol. 35, 1452-1464.

Tedesco, S., Doyle, H., Blasco, J., Redmond, G., Sheehan, D., 2010. Oxidative stress and toxicity of gold nanoparticles in *Mytilus edulis*. Aquat Toxicol. 100, 178-186.

Tervonen, K., Waissi, G., Petersen, E.J., Akkanen, J., Kukkonen, J.V., 2010. Analysis of fullerene-C_{60} and kinetic measurements for its accumulation and depuration in *Daphnia magna*. Environ. Toxicol. Chem. 29, 1072-1078.

Trpkovic, A., Todorovic-Markovic, B., Trajkovic, V., 2012. Toxicity of pristine versus functionalized fullerenes: mechanisms of cell damage and the role of oxidative stress. Arch. Toxicol. 86, 1809-1827.

Urbaszek, P., Gajewicz, A., Sikorska, C., Haranczyk, M., Puzyn, T., 2017. Modeling adsorption of brominated, chlorinated and mixed bromo/chloro-dibenzo-*p*-dioxins on C_{60} fullerene using Nano-QSPR. Beilstein J. Nanotechnol 8, 752-761.

Viarengo, A., 1989. Heavy metals in marine invertebrates: mechanisms of regulation and toxicity at the cellular level. Rev. Aquat. Sci. 1, 295-317.

Viarengo, A., Zanicchi, G., Moore, M.N., Orunesu, M., 1981. Accumulation and detoxication of copper by the mussel *Mytilus galloprovincialis* Lam.: A study of the subcellular distribution in the digestive gland cells. Aquat. Toxicol. 1, 147–157.

Viarengo, A., Lowe, D., Bolognesi, C., Fabbri, E., Koehler, A., 2007. The use of biomarkers in biomonitoring: a 2-tier approach assessing the level of pollutant-induced stress syndrome in sentinel organisms. Comp. Biochem. Physiol. C 146, 281-300.

Wullschleger, S., Loewith, R., Hall, M.N., 2006. TOR signaling in growth and metabolism. Cell 124, 471-484.

Zabirnyk, O., Yezhelyev, M., Seleverstov, O., 2007. Nanoparticles as a novel class of autophagy activators. Autophagy 3, 278-281.

Zheng, W., Wang, B., Si, M., Zou, H., Song, R., Gu, J., Yuan, Y., Liu, X., Zhu, G., Bai, J., Bian, J., Liu, Z., 2018. Zearalenone altered the cytoskeletal structure via ER stress-autophagy-oxidative stress pathway in mouse TM4 Sertoli cells. Sci. Rep. 8, 3320.

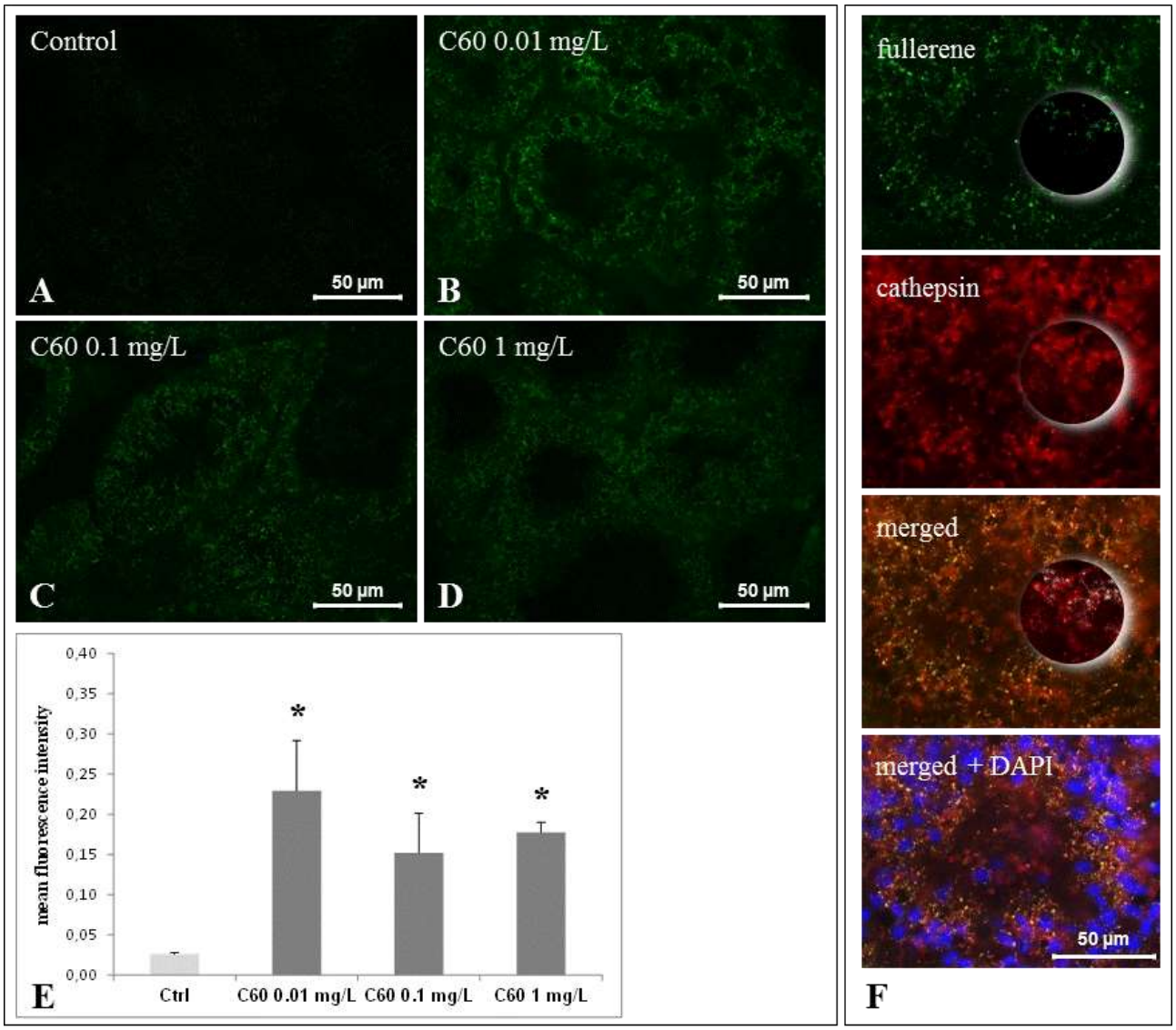
Control
A
50 µm
C60 0.01 mg/L
B
50 µm
C60 0.1 mg/L
C
50 µm
C60 1 mg/L
D
50 µm
mean fluorescence intensity
0,40
0,35
0,30
0,25
0,20
0,15
0,10
0,05
0,00
*
*
*
Ctrl
C60 0.01 mg/L
C60 0.1 mg/L
C60 1 mg/L
E
fullerene
cathepsin
merged
merged + DAPI
50 µm
F

Fig. 1.

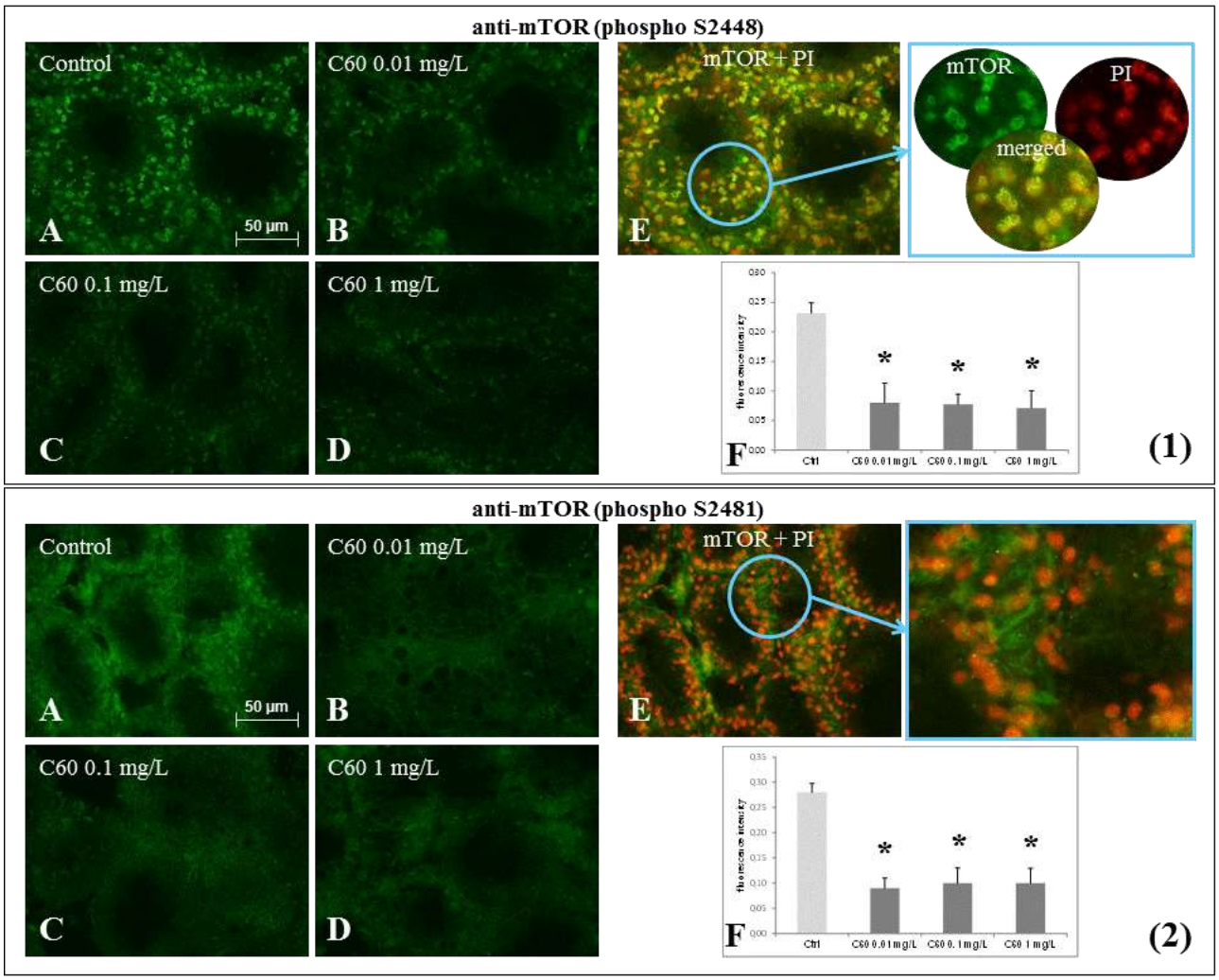
anti-mTOR (phospho S2448)
Control
C60 0.01 mg/L
mTOR + PI
mTOR
PI
merged
A
50 µm
B
E
C60 0.1 mg/L
C60 1 mg/L
C
D
F
(1)
anti-mTOR (phospho S2481)
Control
C60 0.01 mg/L
mTOR + PI
A
50 µm
B
E
C60 0.1 mg/L
C60 1 mg/L
C
D
F
(2)

Fig. 2.

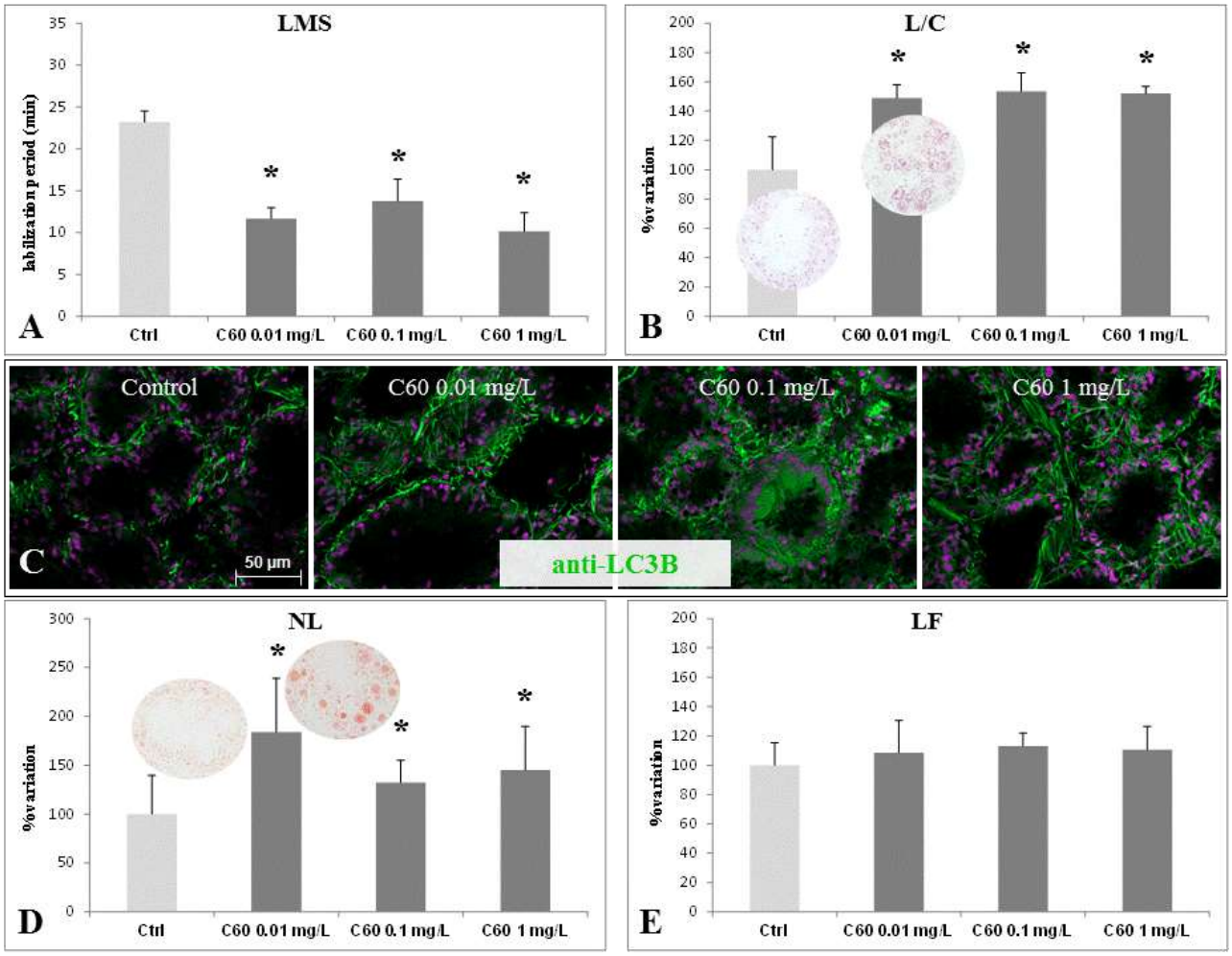
LMS
lahlization period (min)
A
Ctrl
C60 0.01 mg/L
C60 0.1 mg/L
C60 1 mg/L
L/C
%variation
B
Control
C60 0.01 mg/L
C60 0.1 mg/L
C60 1 mg/L
C
50 µm
anti-LC3B
NL
%variation
D
LF
%variation
E

Fig. 3.

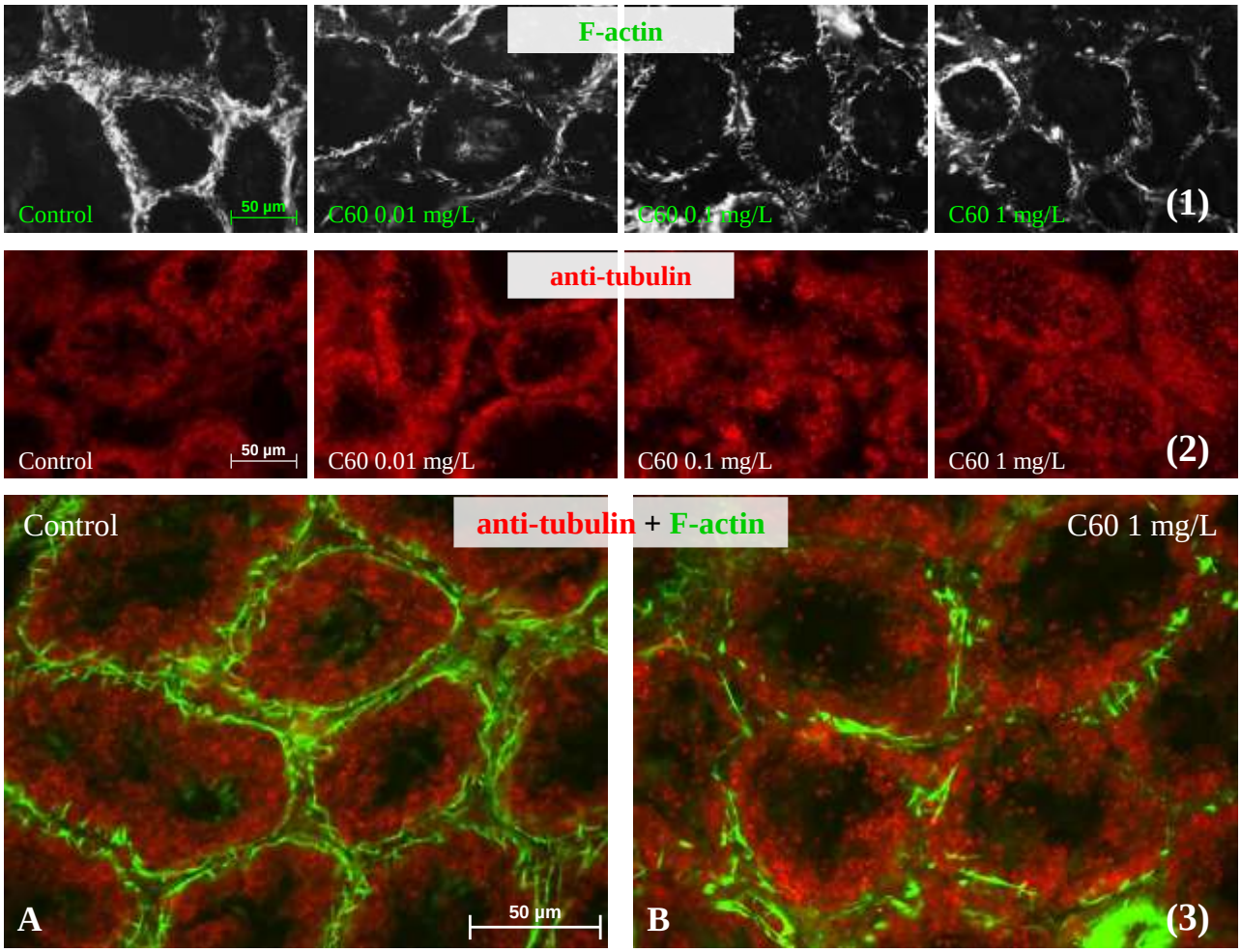
F-actin
Control
50 µm
C60 0.01 mg/L
C60 0.1 mg/L
C60 1 mg/L
(1)
anti-tubulin
Control
50 µm
C60 0.01 mg/L
C60 0.1 mg/L
C60 1 mg/L
(2)
Control
anti-tubulin + F-actin
C60 1 mg/L
A
50 µm
B
(3)

Fig. 4.

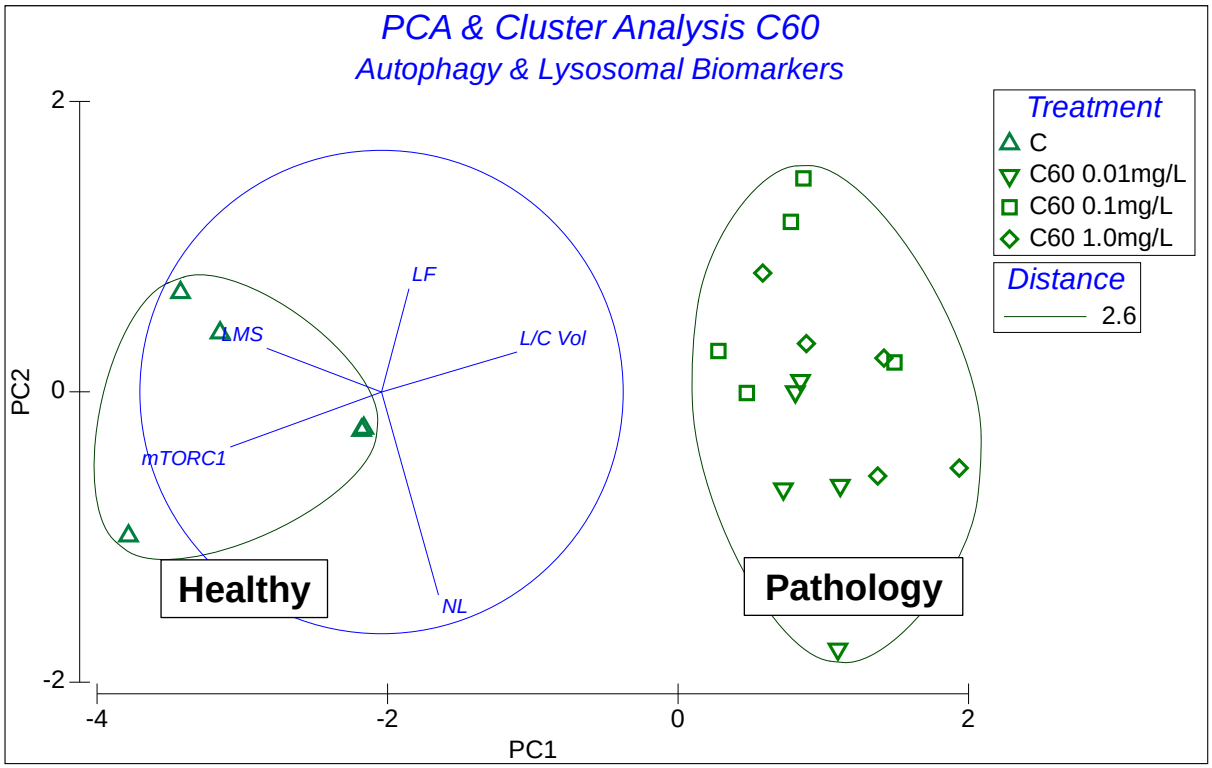
PCA & Cluster Analysis C60
Autophagy & Lysosomal Biomarkers
Treatment
C
C60 0.01mg/L
C60 0.1mg/L
C60 1.0mg/L
Distance
2.6
LF
AMS
L/C Vol
mTORC1
NL
Healthy
Pathology
PC2
PC1
2
0
-2
-4
-2
0
2

Fig. 5.

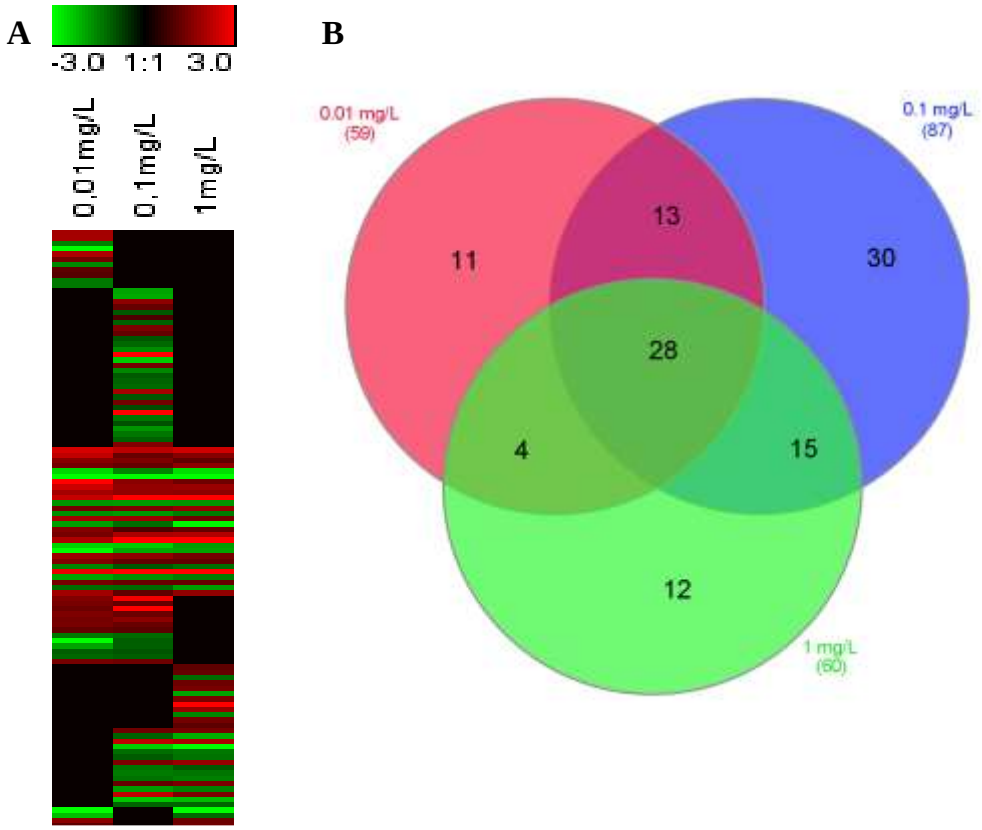
A
-3.0 1:1 3.0
0,01mg/L
0,1mg/L
1mg/L
B
0.01 mg/L
(59)
0.1 mg/L
(87)
1 mg/L
(60)
11
13
30
28
4
15
12

Fig. 6.

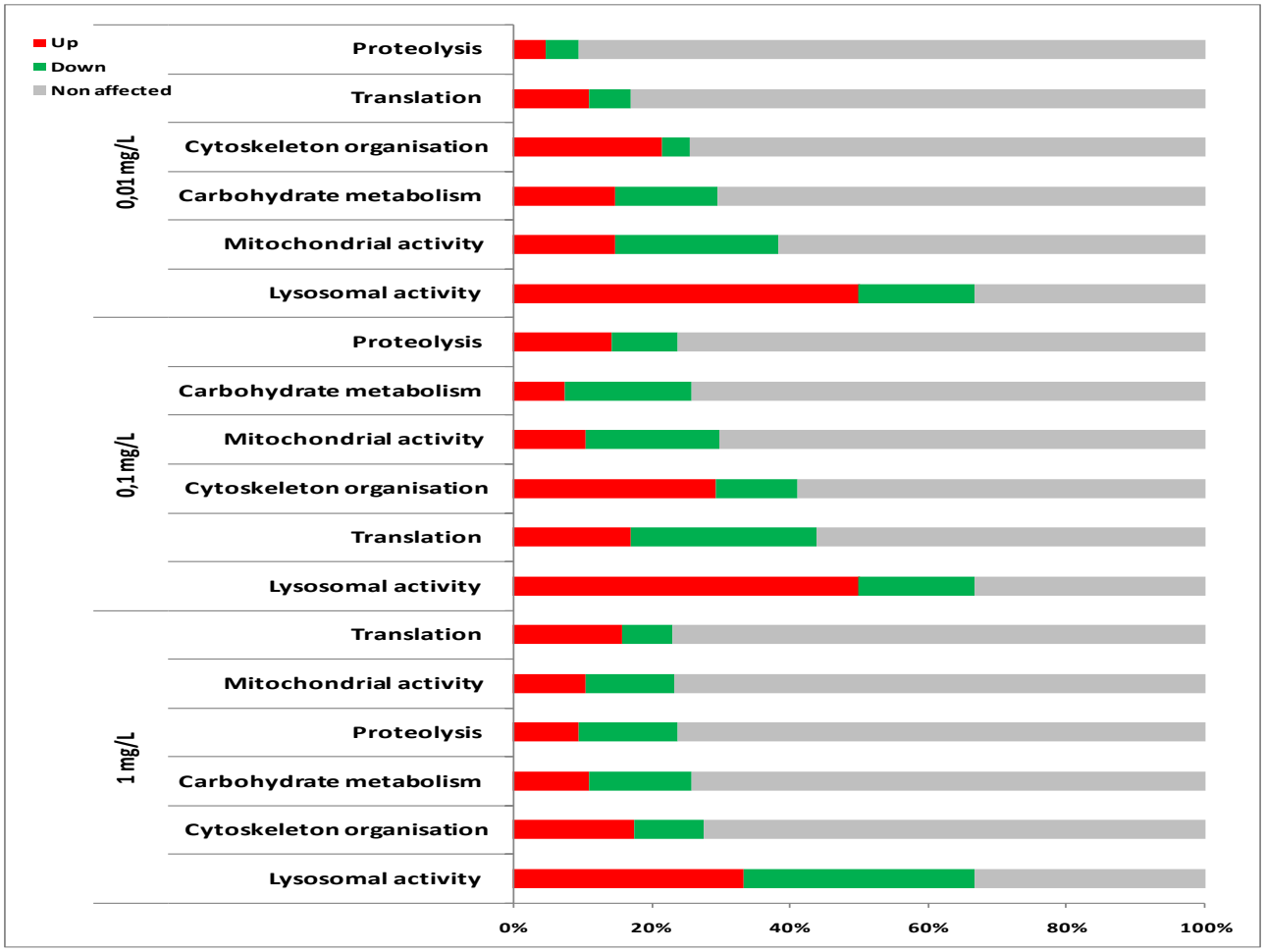
Up
Down
Non affected
0,01 mg/L
Proteolysis
Translation
Cytoskeleton organisation
Carbohydrate metabolism
Mitochondrial activity
Lysosomal activity
0,1 mg/L
Proteolysis
Carbohydrate metabolism
Mitochondrial activity
Cytoskeleton organisation
Translation
Lysosomal activity
1 mg/L
Translation
Mitochondrial activity
Proteolysis
Carbohydrate metabolism
Cytoskeleton organisation
Lysosomal activity
0%
20%
40%
60%
80%
100%

Fig. 7.

Fig. 1. Anti-C_{60} Fullerene immunohistochemical staining (green: FITC conjugated secondary antibody) of digestive gland tissue sections from mussels exposed to different experimental conditions (A: Control; B: 0.01 mg/L C_{60}; C: 0.1 mg/L C_{60}; D: 1 mg/L C_{60}). E) Quantitative fluorescence analysis of anti-C_{60} immunoreaction. Data are mean ± SD of at least five replicates; * = $p < 0.05$ (Mann-Whitney *U*-test). F) Double immunohistochemical staining of digestive glands from mussels exposed to 0.01 mg/L C_{60} fullerene with anti-C_{60} and -cathepsin D antibodies (separate colour images for fullerene (FITC, green) and cathepsin D (DyLight594, red) immunoreactivity were merged into a composite image, whereby the colocalization of both antigens resulted in a yellow colour); in the last picture, nuclei were stained with DAPI (blue).

Fig. 2. Anti-mTOR phospho S2448 (mTORC1) (Panel 1) and anti-mTOR phospho S2481 (mTORC2) (Panel 2) immunohistochemical staining (green: Chromeo conjugated secondary antibody) of digestive gland tissue sections from mussels exposed to different experimental conditions (A: Control; B: 0.01 mg/L C_{60}; C: 0.1 mg/L C_{60}; D: 1 mg/L C_{60}). E) Anti-phospho mTOR (green: Chromeo) and propidium iodide (PI, red) double staining in sections of digestive glands from control mussels. (Panel 1) the anti-mTOR phospho S2448 (mTORC1) fluorescence is located mainly in the perinuclear region of the tubule epithelial cells (yellow colour in the composite image); (Panel 2) the anti-mTOR phospho S2481 (mTORC2) fluorescence is located in the cytoplasm. F) Quantitative fluorescence analysis of anti-mTORC1 (Panel 1) and anti-mTORC2 (Panel 2) immunoreaction. Data are mean ± SD of at least five replicates; * = $p < 0.05$ (Mann-Whitney *U*-test).

Fig. 3. Lysosomal responses in digestive gland of mussels exposed to C_{60} (0.01, 0.1, 1 mg/L): A) Lysosomal membrane stability (LMS); B) lysosomal/cytoplasmic volume ratio (L/C); C) anti-LC3B immunohistochemical staining (green: Alexa Fluor® 488 conjugated secondary antibody; violet:

DAPI nuclear staining; D) neutral lipid accumulation (NL); E) lipofuscin content (LF). Data represent the mean ± SD of at least five replicates. * indicates statistically significant differences ($p < 0.05$ Mann-Whitney *U*-test).

Fig. 4. (Panel 1) F-actin cytoskeleton fluorescent staining by Green Fluorescent Phalloidin Conjugate (greyscale images) and (Panel 2) immunofluorescent anti-tubulin staining (red: DyLight® 594 conjugated secondary antibody) of digestive gland tissue sections from mussels exposed to different experimental conditions (Control, C_{60} 0.01 mg/L, C_{60} 0.1 mg/l, C_{60} 1 mg/L); (Panel 3) antibody to tubulin (red) and F-actin (green) combination staining of tissues sections of Controls (A) and C_{60} 1 mg/L exposed mussels (B).

Fig. 5. Principal component and cluster analysis for the five autophagy/lysosomal function related biomarkers. Vectors are shown for lysosomal membrane stability (LMS), lipofuscin (LF), lysosomal triglyceride (NL), active form (phosphorylated) of the mechanistic target for rapamycin complex 1 cell signalling system (p-mTORC1), and lysosomal/cytoplasmic volume ratio (L/C Vol). Healthy and diseased (pathology) regions of the “health status space” are indicated. PC1 captured 69.6% of the variation.

Fig. 6. Digestive gland expression level profiles of mussels exposed to three increasing concentrations of C_{60} fullerene against controls. A) The heat map (Pearson correlation, complete linkage algorithm) reports the log2 relative expression level with respect to reference condition. 113 differentially expressed genes were generated in at least one condition. B) Venn diagram representation of gene expression patterns clearly depicted that 28 differentially expressed genes (DEGs) are shared between the three species. All DEGs are obtained with respect to the control

condition. Data used to create the Venn-diagram were obtained from microarray analysis. Four biological replicates were considered.

Fig. 7. Over-representation analysis of DEGs in the digestive gland of mussels exposed to C_{60} (0.01 mg/L, 0.1 mg/L and 1 mg/L). Showed are: experimental conditions; biological processes; percentage of up- and down-regulated genes. The over-represented biological processes in C_{60} exposed animals versus control.